

Quantum energies of BPS vortices in $D = 2 + 1$ and $D = 3 + 1$

N. Graham^{a)}, H. Weigel^{b)}

^{a)}*Department of Physics, Middlebury College Middlebury, VT 05753, USA*

^{b)}*Institute for Theoretical Physics, Physics Department,
Stellenbosch University, Matieland 7602, South Africa*

We consider vortices in scalar electrodynamics and compute the leading quantum correction to their energies for the BPS case with identical masses of the Higgs and gauge fields. In particular we focus on the winding number n dependence of these corrections, from which we can extract the binding energies of configurations with larger n . For both dimensionalities, $D = 2 + 1$ and $D = 3 + 1$, we find that quantum corrections decrease approximately linearly with n so that combined vortices are favored over isolated ones.

I. INTRODUCTION

The Abrikosov-Nielsen-Olesen (ANO) vortex [1–3] provides the simplest examples of a topological soliton with integer winding number, relevant to applications in condensed matter [4], particle physics [5] and cosmology [6, 7]. It arises as a classical solution to the field equations in a theory of scalar electrodynamics with spontaneous symmetry breaking, where the scalar can be the field of Cooper pairs in a superconductor or a Higgs-like field in a particle physics model or a cosmic string coupled to a domain wall. After spontaneous symmetry breaking, both the scalar and gauge fields have nonzero mass, and for string configurations that are localized in a two-dimensional transverse plane, the magnetic flux through the plane corresponds to a conserved topological winding number. In the Bogomolny-Prasad-Sommerfeld (BPS) [8, 9] case of equal masses, which we will focus on here, the classical energy is directly proportional to this flux.

Given this classical field theory picture, it is natural to ask how these results are modified by quantum corrections. In particular, it is interesting to see whether or not the above mentioned proportionality will be maintained once these corrections will have been included. To one loop, these corrections consist of the vacuum polarization energy (VPE), the renormalized sum over the zero-point energies $\frac{1}{2}\hbar\omega$ for small oscillations around the classical background. Formally the VPE is defined as

$$\Delta E = \frac{\hbar}{2} \sum_k \left[\omega_k - \omega_k^{(0)} \right] \Big|_{\text{ren.}}, \quad (1)$$

where ω_k and $\omega_k^{(0)}$ denote the spectra of the quantum fluctuations with and without the vortex background, respectively. The subscript indicates that this divergent sum requires renormalization, which is the primary challenge for the calculation.

Let us briefly explain the renormalization procedure. In the background of a static localized configuration we express the renormalized VPE as the sum

$$\Delta E = E_{\text{b.s.}} + \frac{1}{2} \int_0^\infty dk \sqrt{k^2 + M^2} \left(\Delta\rho(k) - \Delta\rho^{(1)}(k) - \Delta\rho^{(2)}(k) \dots \right) + E_{\text{FD}} + E_{\text{CT}} \quad (2)$$

where we have chosen natural units with $\hbar = c = 1$. Here $E_{\text{b.s.}}$ is the contribution from the discrete bound states from the potential induced by the background. The contribution from the continuum scattering states is the momentum integral. The effect of the background is to change the density of states. We call this change $\Delta\rho(k)$. It has a Born expansion in the strength of the potential and subtracting sufficiently many leading orders of this expansion renders the momentum integral finite. In Ref. [10] we have described how this integral combines with $E_{\text{b.s.}}$ when using analytic properties of scattering data and integrating along the imaginary momentum axis. The subtracted pieces are added back in as Feynman diagrams, E_{FD} , that arise from an equivalent expansion of the effective action. When combined with standard counterterms, E_{CT} , the sum $E_{\text{FD}} + E_{\text{CT}}$ is also finite.

We will use scattering theory to compute the change in the density of states and its Born expansion in a partial wave expansion [11]. Here an additional complication arises as a result of the gauge field winding: scattering theory requires that the background fields vanish at spatial infinity, but for string configurations the gauge field is nontrivial, reflecting the topological winding. To remove this behavior, we use a gauge transformation that makes the fields trivial at infinity, at the cost of introducing a singularity in the gauge field at the origin. The associated magnetic field is unchanged, and remains zero at infinity and finite at the origin. This singularity does not contribute to the final

result since it is a gauge artifact, but careful regularization is required to implement it consistently while maintaining gauge symmetry [12].

The first complete treatment of this problem was given in Ref. [13]. There, a more *ad hoc* scheme was used to subtract and add back in terms corresponding to both the renormalization counterterms and the gauge singularity. While in principle the calculations should be equivalent, our approach provides a more systematic separation of the divergences, in the process demonstrating that, surprisingly, a much larger number of partial waves are needed to obtain the large k behavior of $\Delta\rho(k)$ that is consistent with that obtained from analyzing Feynman diagrams. This effect explains the discrepancies between our results and previous calculations, some of which appeared to converge without renormalization [14, 15] when too few partial waves are taken into account; including a larger number of partial waves restores the expected divergence.

In this paper we consider vortices in both $D = 2 + 1$ and $D = 3 + 1$ spacetime dimensions. In the former case, the lower dimension means fewer diagrams are divergent, as is typical in quantum field theory. We nonetheless include finite counterterms to implement the same on-shell renormalization conditions as in $3 + 1$ dimensions in which the location and residue of the propagator poles, corresponding to the mass and normalization of single-particle states, are left unchanged. (While in the general case the mass ratio could be affected by quantum corrections, the BPS condition continues to hold in the quantum theory and ensures that the masses remain equal.) In the case of $3 + 1$ dimensions, the scattering density of states remains the same, but we must use analytic continuation to consistently include the integral over the momentum in the trivial direction [16].

Since the classical BPS vortex has energy proportional to its winding number, the classical energy of a winding n vortex is equal to the energy of n isolated vortices. In the condensed matter system, it represents the boundary between Type I and Type II superconductors. The quantum correction will therefore either stabilize or destabilize the higher winding configurations; by carrying out the calculation through $n = 4$ we find that higher winding is stabilized.

Throughout the paper we treat the $D = 2 + 1$ and $D = 3 + 1$ cases in parallel without introducing separate notations, use the context to identify the particular case. In Section II we introduce the classical vortex configuration in singular gauge. The quantization of the theory at one loop and the corresponding on-shell renormalization procedure are described in Sections III and IV, respectively. In Section V we explain the computation of the VPE using scattering data on the imaginary momentum axis and show how we move the divergent contributions from that momentum integral into Feynman diagrams, which are then combined with the counterterms from Section IV. Numerical results are presented and discussed in Section VI and we give a short summary and conclusion in chapter VII.

II. CLASSICAL SOLUTIONS

We start from the Lagrangian

$$\mathcal{L} = -\frac{1}{4}F_{\mu\nu}F^{\mu\nu} + |D_\mu\Phi|^2 - \frac{\lambda}{4}(|\Phi|^2 - v^2)^2, \quad (3)$$

where as usual $F_{\mu\nu} = \partial_\mu A_\nu - \partial_\nu A_\mu$ and $D_\mu\Phi = (\partial_\mu - ieA_\mu)\Phi$ for an Abelian gauge theory.

In singular gauge the profiles associated with winding number n are the functions $g(\rho)$ and $h(\rho)$ within the ansätze

$$\Phi_S = v h(\rho) \quad \text{and} \quad \mathbf{A}_S = n v \hat{\boldsymbol{\varphi}} \frac{g(\rho)}{\rho}, \quad (4)$$

where $\rho = evr$ is dimensionless while r is the physical coordinate. Here $g(\rho)$ ranges from 0 to 1 and $h(\rho)$ ranges from 1 to 0 as ρ goes from 0 to ∞ .

This field configuration leads to the energy functional

$$E_{\text{cl}} = 2\pi v^2 \int_0^\infty \rho d\rho \left[\frac{n^2}{2} \frac{g'^2}{\rho^2} + h'^2 + n^2 \frac{h^2}{\rho^2} g^2 + \frac{\lambda}{4e^2} (h^2 - 1)^2 \right], \quad (5)$$

where primes denote derivatives with respect to ρ . In $D = 2 + 1$, where v^2 has dimensions of mass, E_{cl} is the vortex energy, while in $D = 3 + 1$, where v has dimensions of mass, it is the energy per unit length of the vortex.

Recalling that $M_H^2 = \lambda v^2$ and $M_A^2 = 2v^2 e^2$, the coefficient of the last terms becomes

$$\frac{\lambda}{4e^2} = \frac{M_H^2}{2M_A^2}.$$

That is, when measured in units of $2\pi v^2$, the classical energy only depends on the ratio of the two masses.

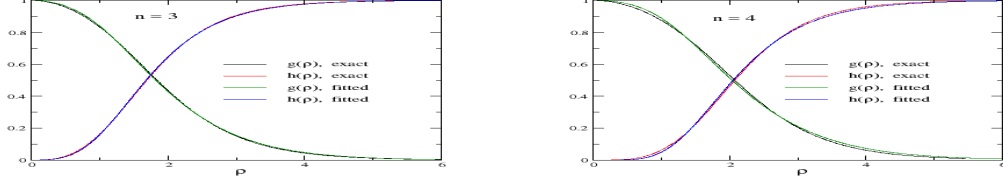


FIG. 1: Comparison of exact and fitted profile functions (from Eq. (9) and table I) for winding numbers $n = 3$ and $n = 4$.

In the BPS case, which we assume henceforth, the coupling constants are related by $\lambda = 2e^2$, *i.e.* $M_H = M_A = M$. Then the energy functional can be written as sums of non-negative quantities plus a surface contribution

$$E_{\text{cl}} = 2\pi v^2 \int_0^\infty \rho d\rho \left\{ \frac{1}{2} \left[\frac{n}{\rho} g' - (h^2 - 1) \right]^2 + \left[h' - \frac{n}{\rho} gh \right]^2 \right\} + 2\pi n v^2 g(h^2 - 1) \Big|_0^\infty. \quad (6)$$

Hence the minimal energy is fully determined by the asymptotic profiles, yielding $E_{\text{cl}} = 2\pi n v^2 = 2\pi n \frac{M^2}{\lambda}$. These profiles obey the first-order differential equations

$$g' = \frac{\rho}{n} (h^2 - 1) \quad \text{and} \quad h' = \frac{n}{\rho} gh, \quad (7)$$

with the boundary conditions

$$h(0) = 1 - g(0) = 0 \quad \text{and} \quad \lim_{\rho \rightarrow \infty} h(\rho) = 1 - \lim_{\rho \rightarrow \infty} g(\rho) = 1, \quad (8)$$

which correspond to field configurations that are coordinate independent at spatial infinity. The topological structure appears through a singularity in the gauge field at the origin, while the magnetic field remains finite everywhere. We have solved the differential equations in (7) numerically, but for later use in the scattering problem an approximate expression in terms of elementary functions is very helpful. It turns out that for $1 \leq n \leq 4$ the correlation coefficients for the fit

$$h(\rho) = \alpha_2 \tanh^n(\alpha_1 \rho) + [1 - \alpha_2] \tanh^n(\alpha_0 \rho) \quad \text{and} \quad g(\rho) = \beta_1 \rho \frac{1 - \tanh^2(\beta_2 \rho)}{\tanh(\beta_1 \rho)} \quad (9)$$

with the fit parameters α_i and β_i listed in Table I deviate from unity by 10^{-4} or less from the numerical solutions to Eq. (7). The quality of the parameterization is also reflected by the smallness of the relative error $\delta E = E_{\text{fit}}/(2\pi n v^2) - 1$ that is also presented in Tab. I. This accuracy test indicates that the agreement is excellent for $n = 1$ and $n = 2$, but

n	α_0	α_1	α_2	β_1	β_2	δE
1	0.8980	0.6621	0.1890	0.5361	0.7689	4.2×10^{-6}
2	0.9072	0.8288	2.6479	1.0949	0.8042	1.9×10^{-5}
3	0.8290	0.7882	5.1953	1.1328	0.7425	1.5×10^{-3}
4	0.7755	0.7350	5.2009	1.1034	0.6853	5.6×10^{-3}

TABLE I: Fit parameters for vortex profiles. The quality of the fit is estimated by the accuracy of the energy: $\delta E = E_{\text{fit}}/(2\pi v^2) - 1$, where E_{fit} is obtained by substituting (9) into Eq. (5).

merely good for $n = 3$ and $n = 4$. To show that the fit is nevertheless also suitable in these cases, we display the corresponding profiles in Figure 1. A graphical comparison for $n = 1$ and $n = 2$ does not provide visible differences and we refrain from its presentation.

III. QUANTIZATION

In this section we quantize the theory, including the relevant ghost fields required for gauge fixing, derive the equations of motion for the harmonic fluctuations, and construct the renormalization counterterms.

A. Lagrangian for fluctuations

We introduce time dependent fluctuations about the vortex via

$$\Phi = \Phi_S + \eta \quad \text{and} \quad A^\mu = A_S^\mu + a^\mu \quad (10)$$

and extract the harmonic terms after several integrations by parts as

$$\begin{aligned} \mathcal{L}^{(2)} = & -\frac{1}{2} (\partial_\mu a_\nu) (\partial^\mu a^\nu) + \frac{1}{2} (\partial_\mu a^\mu)^2 + |\Phi_S|^2 a_\mu a^\mu \\ & + |D_\mu \eta|^2 - (|\Phi_S|^2 - 1) |\eta|^2 - \frac{1}{2} (\Phi_S \eta^* + \Phi_S^* \eta)^2 \\ & + i (\Phi_S \eta^* - \Phi_S^* \eta) \partial_\mu a^\mu + 2i a^\mu (\eta^* D_\mu \Phi_S - \eta D_\mu^* \Phi_S^*) a^\mu, \end{aligned} \quad (11)$$

where D_μ is the covariant derivative with the vortex configuration \mathbf{A}_S substituted, $D_0 = \partial_t$ and $\mathbf{D} = \nabla + i n \boldsymbol{\varphi} \frac{g(\rho)}{\rho}$, and we have chosen units with $ev = 1$ such that both particles have mass $\sqrt{2}$. The gauge is fixed from the vortex background by adding an R_ξ (with $\xi = 1$) type Lagrangian that cancels the $\partial_\mu a^\mu$ term,

$$\mathcal{L}_{\text{gf}} = -\frac{1}{2} [\partial_\mu a^\mu + i (\Phi_S \eta^* - \Phi_S^* \eta)]^2. \quad (12)$$

Collecting the harmonic terms yields

$$\mathcal{L}^{(2)} + \mathcal{L}_{\text{gf}} = -\frac{1}{2} (\partial_\mu a_\nu) (\partial^\mu a^\nu) + |\Phi_S|^2 a_\mu a^\mu + |D_\mu \eta|^2 - (3|\Phi_S|^2 - 1) |\eta|^2 + 2i a^\mu (\eta^* D_\mu \Phi_S - \eta D_\mu^* \Phi_S^*). \quad (13)$$

We still have to subtract the ghost contribution to the VPE associated with the gauge fixing in Eq. (12), which we write as $\mathcal{L}_{\text{gf}} = -\frac{1}{2} G^2$. The infinitesimal gauge transformations reads

$$A^\mu \rightarrow A^\mu + \partial_\mu \chi, \quad \Phi_0 + \eta \rightarrow \Phi_0 + \eta + i\chi(\Phi_0 + \eta) \quad \text{so that} \quad \eta \rightarrow \eta + i\chi(\Phi_0 + \eta). \quad (14)$$

Then

$$\left. \frac{\partial G}{\partial \chi} \right|_{\chi=0} = \partial_\mu \partial^\mu + (2|\Phi_0|^2 + \Phi_0 \eta^* + \Phi_0^* \eta). \quad (15)$$

This induces the ghost Lagrangian (in agreement with Refs. [17, 18])

$$\mathcal{L}_{\text{gh}} = -\partial_\mu \bar{c} \partial^\mu c + 2|\Phi_0| \bar{c} c + \text{non-harmonic terms}. \quad (16)$$

Its VPE is (the negative of) that of a Klein Gordon field of mass $\sqrt{2}$ in the background potential $2(h^2 - 1)$, which can be easily computed. Of course, it must be subtracted with a factor of two from the above. Note from Eq. (13) that the non-transverse components of a_μ couple to the same background potential.

In $D = 2 + 1$ the spectrum consists of four real decoupled fields with mass $\sqrt{2}$: a_1 , a_2 , $\text{Re}(\eta)$ and $\text{Im}(\eta)$. Three other fields, also with mass $\sqrt{2}$, are fully decoupled: a_0 and the two ghosts. The ghosts count negatively, and one of them cancels against the temporal component of the gauge field. In total there are then $5 - 2 = 3$ physical degrees of freedom. When computing the VPE we thus have to subtract a boson type contribution from the background $2(h^2 - 1)$. In $D = 3 + 1$ the gauge field has an additional decoupled longitudinal component so that the non-transverse and ghost contributions cancel completely and we only need to consider a_1 and a_2 together with the complex Higgs field.

B. Wave-equations for quantum fluctuations

To formulate the scattering problem, we employ a partial wave decomposition using the complex combinations

$$a_x + ia_y = \sqrt{2} i e^{-i\omega t} \sum_\ell a_\ell(\rho) e^{i\ell\varphi} \quad \text{and} \quad \eta = e^{-i\omega t} \sum_\ell \eta_\ell(\rho) e^{i\ell\varphi}. \quad (17)$$

We have an analogous expansion for $a_x - ia_y$ and η^* and, in general, a coupled system for four radial functions. In the BPS case, fortunately, this system decouples into two sub-blocks, with the one containing $a_x - ia_y$ and η^* being identical to the above. It will then suffice to solve

$$\begin{aligned} \frac{1}{\rho} \frac{\partial}{\partial \rho} \rho \frac{\partial}{\partial \rho} \eta_\ell(\rho) &= -q^2 \eta_\ell(\rho) + \left[\frac{\ell^2 - 2n\ell g(\rho) + n^2 g^2(\rho)}{\rho^2} + 3(h^2(\rho) - 1) \right] \eta_\ell(\rho) + \sqrt{2} d(\rho) a_{\ell+1}(\rho) \\ \frac{1}{\rho} \frac{\partial}{\partial \rho} \rho \frac{\partial}{\partial \rho} a_{\ell+1}(\rho) &= -q^2 a_{\ell+1}(\rho) + \left[\frac{(\ell+1)^2}{\rho^2} + 2(h^2(\rho) - 1) \right] a_{\ell+1}(\rho) + \sqrt{2} d(\rho) \eta_\ell(\rho) \end{aligned} \quad (18)$$

with $q^2 = \omega^2 - 2$ and double its VPE. The off-diagonal coupling is $d(\rho) = \frac{\partial h(\rho)}{\partial \rho} + \frac{n}{\rho} h(\rho) g(\rho)$.

As just mentioned the ghost field fully decouples and has a partial wave expansion analog to the Higgs field in Eq. (17),

$$\frac{1}{\rho} \frac{\partial}{\partial \rho} \rho \frac{\partial}{\partial \rho} \zeta_\ell(\rho) = -q^2 \zeta_\ell(\rho) + \left[\frac{\ell^2}{\rho^2} + 2(h^2(\rho) - 1) \right] \zeta_\ell(\rho). \quad (19)$$

IV. RENORMALIZATION

In this section we describe the renormalization of the one-loop corrections arising from the fluctuations about the vortex. We begin by analyzing the effective action.

A. Effective actions in $D = 2 + 1$ and $D = 3 + 1$

To identify the ultraviolet divergences in the form of Feynman diagrams [19, 20], we consider the Lagrangian

$$\mathcal{L} = \frac{1}{2} (\partial_\mu \phi) (\partial^\mu \phi^\dagger) - \frac{1}{2} \phi M^2 \phi^\dagger - \phi V \phi^\dagger \quad (20)$$

with four real fields $\phi = (\eta_1, \eta_2, a_x, a_y)$. The Cartesian components of the gauge fields have been defined in Eq. (17) above, while $\eta = (\eta_1 + i\eta_2)/\sqrt{2}$. We then Taylor expand the effective action for these real scalar fields as

$$\begin{aligned} \mathcal{A}_{\text{eff}} &= \frac{i}{2} \text{Tr} [\partial^2 + M^2 - i0^+ + 2V] \\ &= \mathcal{A}_{\text{eff}}^{(0)} + i \text{Tr} [\hat{G} V] - i \text{Tr} [\hat{G} V \hat{G} V] + \frac{4i}{3} \text{Tr} [\hat{G} V \hat{G} V \hat{G} V] - 2i \text{Tr} [\hat{G} V \hat{G} V \hat{G} V \hat{G} V] + \dots, \end{aligned} \quad (21)$$

where $\hat{G} = (\partial^2 + M^2 - i0^+)^{-1}$ times the 4×4 unit matrix. The functional trace is over the space coordinates as well as the elements of ϕ . The ellipsis in Eq. (21) represents ultra-violet finite terms. The potential matrix is given by $V = V_0 + V_1 + V_2$ with

$$V_0 = e^2 \begin{pmatrix} \frac{3}{2} (\Phi_S^2 - v^2) & 0 & \sqrt{2} \hat{\mathbf{x}} \cdot \mathbf{A}_S \Phi_S & \sqrt{2} \hat{\mathbf{y}} \cdot \mathbf{A}_S \Phi_S \\ 0 & \frac{3}{2} (\Phi_S^2 - v^2) & -(\sqrt{2}/e) \hat{\mathbf{x}} \cdot \nabla \Phi_S & -(\sqrt{2}/e) \hat{\mathbf{y}} \cdot \nabla \Phi_S \\ \sqrt{2} \hat{\mathbf{x}} \cdot \mathbf{A}_S \Phi_S & -(\sqrt{2}/e) \hat{\mathbf{x}} \cdot \nabla \Phi_S & (\Phi_S^2 - v^2) & 0 \\ \sqrt{2} \hat{\mathbf{y}} \cdot \mathbf{A}_S \Phi_S & -(\sqrt{2}/e) \hat{\mathbf{y}} \cdot \nabla \Phi_S & 0 & (\Phi_S^2 - v^2) \end{pmatrix} \quad (22)$$

and

$$V_1 = e \begin{pmatrix} 0 & 1 & 0 & 0 \\ -1 & 0 & 0 & 0 \\ 0 & 0 & 0 & 0 \\ 0 & 0 & 0 & 0 \end{pmatrix} \mathbf{A}_S \cdot \nabla \quad \text{and} \quad V_2 = \frac{e^2}{2} \begin{pmatrix} 1 & 0 & 0 & 0 \\ 0 & 1 & 0 & 0 \\ 0 & 0 & 0 & 0 \\ 0 & 0 & 0 & 0 \end{pmatrix} \mathbf{A}_S \cdot \mathbf{A}_S \quad (23)$$

Here we have separated out V_1 and V_2 because they relate to the singular terms in the scattering problem, while V_0 is the 4×4 representation of the non-singular terms in Eq. (18). The renormalization program via Feynman diagrams in dimensional regularization is carried out with the full potential matrix V , while the subtractions that we have indicated in Eq. (2) should only involve V_0 supplemented by the wave-function renormalization of the gauge boson, which is simplified by the fake boson trick described below.

B. On-shell renormalization counterterms

The counterterm Lagrangian has four terms,

$$\mathcal{L}_{\text{CT}} = C_g F_{\mu\nu} F^{\mu\nu} + C_h |D_\mu \Phi|^2 + C_0 (\Phi^2 - v^2) + C_V (\Phi^2 - v^2)^2. \quad (24)$$

The C_0 counterterm arises from varying the vacuum expectation value v in the original Lagrangian, Eq. (3) and the coefficient is chosen such that it exactly cancels $i\text{Tr} [\hat{G}V_0]$ in Eq. (21). This is the no-tadpole condition. The coefficients C_g and C_h are determined such that the residues of the propagators have no quantum correction while C_V is fixed such that the pole position of the Higgs propagator (which determines its mass) does not change at one-loop order. Note that then the pole of the gauge field propagator is a prediction, which in this case is fixed at its classical value by the BPS condition.

In what follows, D will be the physical dimension while D_ϵ occurs in dimensional regularization. That is, for $D = 3 + 1$ we have $D_\epsilon = 4 - 2\epsilon$ and $\epsilon \searrow 0$.

Let us first calculate C_h and C_V in $D = 3 + 1$. For this we need to add the pieces that are quadratic in V_0 from Eq. (21) to these counterterms

$$\begin{aligned} \mathcal{A}^{(V_0)} = & c_V \int d^4x (\Phi_S^2 - v^2)^2 - \frac{13e^4}{32\pi^2} \int \frac{d^4k}{(2\pi)^4} \tilde{v}_H(k) \tilde{v}_H(-k) \int_0^1 dx \ln \left[1 - x(1-x) \frac{k^2}{M^2} \right] \\ & + c_h \int d^4x |D_\mu \Phi|^2 - \frac{1}{8\pi^2} \int \frac{d^4k}{(2\pi)^4} \text{tr} [\tilde{a}(k) \tilde{a}^\dagger(-k)] \int_0^1 dx \ln \left[1 - x(1-x) \frac{k^2}{M^2} \right], \end{aligned} \quad (25)$$

where c_G and c_V are the finite pieces of the counterterm term coefficients that remain after canceling the $1/\epsilon$ singularities from the loop integrals.¹ Furthermore $\tilde{v}_H(k)$ and $\tilde{a}(k)$ are the Fourier transforms of

$$v_H = \Phi_S^2 - v^2 \quad \text{and} \quad a = \sqrt{2}e \begin{pmatrix} e\hat{\mathbf{x}} \cdot \mathbf{A}_S \Phi_S & e\hat{\mathbf{y}} \cdot \mathbf{A}_S \Phi_S \\ -\hat{\mathbf{x}} \cdot \nabla \Phi_S & -\hat{\mathbf{y}} \cdot \nabla \Phi_S \end{pmatrix}, \quad (26)$$

respectively. For example, $\tilde{v}_H(k) = \int d^Dx [\Phi_S^2 - v^2] e^{ik_\mu x^\mu}$. We write $\mathcal{A}^{(V_0)}$ using momentum dependent two-point functions

$$\mathcal{A}^{(V_0)} = \int \frac{d^4k}{(2\pi)^4} \{ \text{tr} [\tilde{a}(k) \tilde{a}^\dagger(-k)] G_H(k^2) + \tilde{v}_H(k) \tilde{v}_H(-k) G_V(k^2) \}. \quad (27)$$

The on-shell renormalization conditions fix c_h and c_V such that $G_H(M^2) = 0$ and $G_V(M^2) = 0$,

$$c_h = \frac{e^2}{4\pi^2} \left(2 - \frac{\pi}{\sqrt{3}} \right) \quad \text{and} \quad c_V = \frac{13e^4}{32\pi^2} \left(\frac{\pi}{\sqrt{3}} - 2 \right). \quad (28)$$

For $D = 2 + 1$ there are two essential differences. First, diagrams with two insertions of V_0 are finite and, second, for C_H we have to include the ghost piece from $-i\text{Tr} [\hat{G}v_H \hat{G}v_H]$, which is also finite. This yields

$$\begin{aligned} \mathcal{A}^{(V_0)} = & C_V \int d^3x (\Phi_S^2 - v^2)^2 + \frac{11e^4}{16\pi M} \int \frac{d^3k}{(2\pi)^3} \tilde{v}_H(k) \tilde{v}_H(-k) \int_0^1 \frac{dx}{\sqrt{1 - x(1-x) \frac{k^2}{M^2}}} \\ & + C_h \int d^3x |D_\mu \Phi|^2 + \frac{1}{4\pi M} \int \frac{d^3k}{(2\pi)^3} \text{tr} [\tilde{a}(k) \tilde{a}^\dagger(-k)] \int_0^1 \frac{dx}{\sqrt{1 - x(1-x) \frac{k^2}{M^2}}}. \end{aligned} \quad (29)$$

The on-shell conditions lead to

$$C_h = \frac{\ln(3)}{4\pi} \frac{e^2}{M} \quad \text{and} \quad C_V = -\frac{11 \ln(3)}{16\pi} \frac{e^4}{M}. \quad (30)$$

¹ These finite pieces vanish in the $\overline{\text{MS}}$ renormalization scheme.

Observe that in comparison with Eq. (25), the relative factor between the coefficients of the momentum integrals has changed from $\frac{13e^4}{4}$ to $\frac{11e^4}{4}$ due to the ghost contribution.

The computation of C_g starts from

$$\mathcal{A}^{(A)} = C_G \int d^3x F_{\mu\nu} F^{\mu\nu} + i\text{Tr} [\hat{G}V_2] - i\text{Tr} [\hat{G}V_1 \hat{G}V_1] \quad (31)$$

For two space dimensions we find

$$\begin{aligned} \mathcal{A}^{(A)} = C_G \int d^3x F_{\mu\nu} F^{\mu\nu} \\ + e^2 \frac{\mu^{3-D_\epsilon}}{(4\pi)^{D_\epsilon/2}} \Gamma\left(1 - \frac{D_\epsilon}{2}\right) \int \frac{d^3k}{(2\pi)^3} \tilde{A}_\mu(k) \tilde{A}^\mu(-k) \int_0^1 dx \left[M^{D_\epsilon-2} - (M^2 - x(1-x)k^2)^{D_\epsilon/2-1} \right], \end{aligned} \quad (32)$$

where $\tilde{A}^\mu(k) = \int d^Dx A^\mu(x) e^{ik_\nu x^\nu}$ denotes the Fourier transform of the gauge field. We have repeatedly used $p_\mu \tilde{A}^\mu(k) = 0$ which results from the vortex property $\partial_\mu A^\mu = 0$ and also implies

$$\int d^3x F_{\mu\nu} F^{\mu\nu} = 2 \int \frac{d^3k}{(2\pi)^3} k^2 \tilde{A}_\mu(k) \tilde{A}^\mu(-k). \quad (33)$$

The residue of the $D_\epsilon = 2$ pole is zero and we can directly substitute $D_\epsilon = 3$,

$$\mathcal{A}^{(A)} = -\frac{e^2 M}{4\pi} \int \frac{d^3k}{(2\pi)^3} \tilde{A}_\mu(k) \tilde{A}^\mu(-k) \int_0^1 dx \left[1 - \sqrt{1 - x(1-x) \frac{k^2}{M^2}} - 4\pi C_g \frac{k^2}{e^2 M} \right]. \quad (34)$$

In the on-shell scheme we demand that the square bracket vanishes for $p^2 = M^2$, so that

$$4\pi C_g \frac{M}{e^2} = \int_0^1 dx \left[1 - \sqrt{1 - x(1-x)} \right] \quad \text{and thus} \quad C_g = \frac{1}{32\pi} [4 - \ln(27)] \frac{e^2}{M}. \quad (35)$$

For the case of three space dimensions Eq. (32) has a pole when we approach $D_\epsilon \rightarrow D = 4$,

$$\begin{aligned} \mathcal{A}_2 = C_g \int d^4x F_{\mu\nu} F^{\mu\nu} - \frac{1}{12} \left(\frac{e}{4\pi} \right)^2 \left[\frac{1}{\epsilon} + 1 - \gamma + \ln \left(\frac{4\pi\mu^2}{M^2} \right) \right] \int d^4x F_{\mu\nu} F^{\mu\nu} \\ - \frac{1}{2} \left(\frac{eM}{4\pi} \right)^2 \int \frac{d^4k}{(2\pi)^4} \tilde{F}_{\mu\nu}(k) \tilde{F}^{\mu\nu}(-k) \int_0^1 dx \frac{1}{k^2} \left[1 - x(1-x) \frac{k^2}{M^2} \right] \ln \left[1 - x(1-x) \frac{k^2}{M^2} \right]. \end{aligned} \quad (36)$$

Observe that we have factored out $1/k^2$ to substitute the momentum space version of Eq. (33). This does not induce any singularity because the logarithm in the Feynman parameter integral behaves like k^2 when $k \rightarrow 0$. The on-shell scheme produces the counterterm coefficient

$$C_g = \frac{1}{12} \left(\frac{e}{4\pi} \right)^2 \left[\frac{1}{\epsilon} - \gamma + \ln \left(\frac{4\pi\mu^2}{M^2} \right) + \frac{3\sqrt{3}\pi - 16}{3} \right]. \quad (37)$$

In the scattering approach, the two terms in Eq. (31) emerge from different orders in the Born series in Eq. (2). Thus the combination that removes the superficial quadratic divergence is difficult to identify. It is more appropriate to treat the cancel the singularity in C_g by the method we describe in the next section.

There are additional superficial divergences in $D = 3 + 1$ when expanding the effective action, Eq. (21). However, the logarithmic divergences from $V_0 \otimes V_2$ and $V_0 \otimes V_1 \otimes V_1$ cancel, as do those from $V_2 \otimes V_2$, $V_2 \otimes V_1 \otimes V_1$ and $V_1 \otimes V_1 \otimes V_1 \otimes V_1$.

C. Fake boson subtraction

To deal with the remaining logarithmic divergence in $D = 3 + 1$, we introduce the fake boson technique, in which we begin by considering bosonic fluctuations about the static potential $V_f(r)$. We take this boson field to be complex

because its scattering data will later be combined with those from the complex vortex fluctuations in Eq. (18). The corresponding second-order effective action is

$$\begin{aligned} \mathcal{A}_2^{(\text{fb})} = & \frac{1}{2(4\pi)^2} \left[\frac{1}{\epsilon} - \gamma + \ln \left(\frac{4\pi\mu^2}{M^2} \right) \right] \int d^4x V_f^2 \\ & - \frac{1}{2(4\pi)^2} \int \frac{d^4k}{(2\pi)^4} \tilde{V}_f(k) \tilde{V}_f(-k) \int_0^1 dx \ln \left[1 - x(1-x) \frac{k^2}{M^2} \right], \end{aligned} \quad (38)$$

with $\tilde{V}(k) = \int d^Dx V(x) e^{ik_\nu x^\nu}$. We define the normalization such that the $1/\epsilon$ in singularities in Eqs. (37) and (38) match. That is,

$$\frac{-6c_B}{e^2} \int \frac{d^4x}{TL} V_f^2 = \int \frac{d^4x}{TL} F_{\mu\nu} F^{\mu\nu} = 4\pi v^2 \int_0^\infty \rho d\rho \left(\frac{n^2 g'^2}{\rho} \right)^2, \quad (39)$$

where TL is the volume of the subspace in which the vortex is translationally invariant. Then we end up with the finite expression

$$\begin{aligned} C_g \int \frac{d^4x}{TL} F_{\mu\nu} F^{\mu\nu} + c_B \mathcal{A}_2^{(\text{fb})} = & \frac{3\sqrt{3}\pi - 16}{144\pi} (ev)^2 \int_0^\infty \rho d\rho \left(\frac{n^2 g'^2}{\rho} \right)^2 \\ & - \frac{c_B}{2(4\pi)^2} \int \frac{d^4k}{(2\pi)^4} \tilde{V}_f(k) \tilde{V}_f(-k) \int_0^1 dx \ln \left[1 - x(1-x) \frac{k^2}{M^2} \right]. \end{aligned} \quad (40)$$

Above we have outlined the fake boson approach for $D = 3 + 1$ where it is needed to remove an ultra-violet divergence. Though it is not required in $D = 2 + 1$, we apply it there as well because the numerical evaluation of the momentum space integrals in Sec. V is more stable with the corresponding subtraction. The correspondingly renormalized part of the action is

$$\begin{aligned} C_g \int d^3x F_{\mu\nu} F^{\mu\nu} + c_B \mathcal{A}_2^{(\text{fb})} = & \frac{e^2 v^2 T}{32\pi M} [4 - \ln(27)] \int_0^\infty \rho d\rho \left(\frac{n^2 g'^2}{\rho} \right)^2 \\ & + \frac{c_B}{16\pi M} \int \frac{d^3k}{(2\pi)^3} \tilde{V}_f(k) \tilde{V}_f(-k) \int_0^1 \frac{dx}{\sqrt{1 - x(1-x) \frac{k^2}{M^2}}}. \end{aligned} \quad (41)$$

V. VACUUM POLARIZATION ENERGY (VPE)

A. Relevance of scattering data

In this section we briefly review the spectral methods for computing the VPE of static, extended field configurations from Ref. [11].

The background field configuration induces a potential for small amplitude fluctuations, which are treated by standard techniques of scattering theory in quantum mechanics. These calculations provide the bound state energies, ω_j , which directly enter the VPE, as well as the phase shifts $\delta(k)$, or more generally the scattering matrix, as functions of the wave-number k for single-particle energies above the threshold given by the mass m of the fluctuating field. Those phase shifts parameterize the change in the density of continuum modes via the Friedel-Krein formula [21],

$$\Delta\rho_\ell = \frac{1}{\pi} \frac{d\delta_\ell(k)}{dk}, \quad (42)$$

where ℓ indexes the partial wave-expansion in Eq. (17). As discussed in Eq. (2) that change determines the continuum contribution to the VPE

$$\Delta E = \frac{1}{2} \sum_j^{\text{b.s.}} \omega_j + \int_0^\infty \frac{dk}{2\pi} \sum_\ell \sqrt{k^2 + m^2} \frac{d\delta_\ell(k)}{dk} + E_{\text{CT}}. \quad (43)$$

Our scattering problem is in two space dimensions and all angular momentum sums run over the integers from negative to positive infinity.

Next we describe how the counterterms cancel the divergences originating from the large k behavior of the phase shift in the momentum integral. In the previous section we have shown that the Feynman diagrams are generated by expanding the effective action in powers of the potential appearing in the scattering wave-equations. The equivalent Born expansion for the phase shift is most efficiently performed within the variable phase approach [22], which factors out the outgoing wave from the full wave-function. We will provide details of that approach for the vortex problem in the next section and restrict ourselves here to the description of the main concepts. The factor function is called the Jost solution $\mathcal{F}_\ell(r, k)$. The differential equation for the Jost solution is (numerically) solved with the boundary condition $\lim_{r \rightarrow \infty} \mathcal{F}_\ell(r, k) = \mathbf{1}$. In a multi-channel problem $\mathcal{F}_\ell(r)$ is matrix-valued. Regularity of the scattering wave-function then determines the scattering matrix and subsequently the phase shift (for a particular partial wave)

$$\delta_\ell(k) = \frac{1}{2i} \ln \det \lim_{r \rightarrow 0} [\mathcal{F}_\ell^*(r, k) \mathcal{F}_\ell^{-1}(r, k)] .$$

Most importantly, the Jost solution has a perturbation expansion in powers of the scattering potential: $\mathcal{F}_\ell(r, k) = \mathbf{1} + \mathcal{F}_\ell^{(1)}(r, k) + \mathcal{F}_\ell^{(2)}(r, k) + \dots$ with boundary conditions $\lim_{r \rightarrow \infty} \mathcal{F}_\ell^{(n)}(r, k) = 0$. The individual contributions can be straightforwardly obtained by iterating the wave-equation. In turn this induces the perturbation expansion, which is the so-called Born series for the phase shift,

$$\begin{aligned} \delta_\ell^{(1)}(k) &= \frac{1}{2i} \lim_{r \rightarrow 0} \text{tr} \left[\mathcal{F}_\ell^{(1)*}(r, k) - \mathcal{F}_\ell^{(1)}(r, k) \right] , \\ \delta_\ell^{(2)}(k) &= \frac{1}{2i} \lim_{r \rightarrow 0} \text{tr} \left[\mathcal{F}_\ell^{(2)*}(r, k) - \mathcal{F}_\ell^{(2)}(r, k) - \frac{1}{2} [\mathcal{F}_\ell^{(1)}(r, k)]^2 + \frac{1}{2} [\mathcal{F}_\ell^{(1)*}(r, k)]^2 \right] , \quad \text{etc..} \end{aligned} \quad (44)$$

Since the phase shift is dimensionless, the expansion in powers of the potential is also an expansion in the inverse momentum. Hence taking sufficiently many terms, say N , from the Born series and subtracting them from the phase shift will render the momentum integral in Eq. (43) finite. We then add these subtractions back in form of the equivalent Feynman expansion up to order N that we developed in the previous section,

$$\Delta E = \frac{1}{2} \sum_j^{\text{b.s.}} \omega_j + \int_0^\infty \frac{dk}{2\pi} \sum_\ell \sqrt{k^2 + m^2} \frac{d}{dk} \left[\delta_\ell(k) - \delta_\ell^{(1)}(k) - \delta_\ell^{(2)}(k) - \dots - \delta_\ell^{(N)}(k) \right] + E_{\text{FD}}^{(N)} + E_{\text{CT}} . \quad (45)$$

The sum $E_{\text{FD}}^{(N)} + E_{\text{CT}}$ combines to form an ultra-violet finite expression as, for example, for the action in Eq. (25).

To further process the momentum integral we recall that the Jost function² $\mathcal{F}(k) = \lim_{r \rightarrow 0} \mathcal{F}(r, k)$ is analytic for $\text{Im}(k) \geq 0$ and that for real k its complex conjugate is $\mathcal{F}^*(k) = \mathcal{F}(-k)$ [23]. Thus we write $\delta_\ell(k) = (1/2i) [\ln \det \mathcal{F}_\ell(-k) - \ln \det \mathcal{F}_\ell(k)]$ and extend the integral over the full real axis. With the Born subtractions made above, there will be no contribution to the integral from a semi-circle at infinitely large $|k|$ for $\text{Im}(k) \geq 0$. We may thus close the contour accordingly. However, we have to circumvent the branch cut that emerges in $\sqrt{k^2 + m^2}$ for $\text{Im}(k) > m$. That will leave a contribution along the imaginary k axis starting at im that picks up the discontinuity of the square root. Finally we collect the residues that emerge from the zeros of the Jost function, which create first-order poles in the logarithmic derivative. These zeros are known [23] to be single and to be located at the wave-numbers corresponding to the bound state energies: $k_j = i\sqrt{m^2 - \omega_j^2}$. By virtue of Cauchy's theorem these residues exactly cancel the discrete bound state contribution in the VPE [24]. Introducing $\nu_\ell(t) = \ln \det \mathcal{F}_\ell(it)$ and integrating by parts, we obtain the compact expression

$$\Delta E = \int_m^\infty \frac{dt}{2\pi} \frac{t}{\sqrt{t^2 - m^2}} \sum_\ell \left[\nu_\ell(t) - \nu_\ell^{(1)}(t) - \nu_\ell^{(2)}(t) - \dots - \nu_\ell^{(N)}(t) \right] + E_{\text{FD}}^{(N)} + E_{\text{CT}} , \quad (46)$$

where the $\nu_\ell^{(n)}(t)$ arise from the Born series expansion of $\mathcal{F}_\ell(it)$.

The situation in $D = 3 + 1$ is slightly more complicated. The vortex is translationally invariant along the symmetry axis (which we choose to be in the z direction). The wave-function has a plane wave factor for the dependence of that coordinate and we have to integrate over the corresponding momentum. Since the phase shifts do not depend on that momentum, there is no Born subtraction that removes the ultra-violet divergence emerging from that integration. The

² The general definition of the Jost function is the Wronskian of the Jost and regular solutions.

solution is the so-called interface formalism developed in Ref. [16], in which the integral is dimensionally regularized in $d - 1$ space dimensions, showing that the divergence is proportional to

$$\frac{1}{d-1} \left\{ \int_0^\infty \frac{dk}{\pi} k^2 \frac{d}{dk} \sum_\ell \left[\delta_\ell(k) - \delta_\ell^{(1)}(k) - \delta_\ell^{(2)}(k) - \dots - \delta_\ell^{(N)}(k) \right] + \sum_j^{\text{b.s.}} \omega_j^2 - m^2 \right\}.$$

The expression in curly brackets actually vanishes in all partial wave channels individually via one of the sum rules that generalize Levinson's theorem [25], which follow from analyticity of the Jost function for $\text{Im}(k) \geq 0$. Thus the limit $d \rightarrow 1$ can be taken, yielding

$$\Delta E = \frac{-1}{8\pi} \left[\int_0^\infty \frac{dk}{\pi} \sum_\ell \omega^2(k) \ln \frac{\omega^2(k)}{\bar{\mu}^2} \frac{d}{dk} \left[\nu_\ell(t) - \nu_\ell^{(1)}(t) - \nu_\ell^{(2)}(t) - \dots - \nu_\ell^{(N)}(t) \right] + \sum_j^{\text{b.s.}} \omega_j^2 \ln \frac{\omega_j^2}{\bar{\mu}^2} \right] + E_{\text{FD}}^{(N)} + E_{\text{CT}} \quad (47)$$

as the VPE per unit length of the vortex. The arbitrary energy scale $\bar{\mu}$ has been introduced for dimensional reasons. It has no effect by the above sum rule in combination with Levinson's theorem. Again, by closing the contour in the upper half k plane we can remove the explicit bound state contribution. This time we pick up the discontinuity from the logarithm,

$$\Delta E = \int_m^\infty \frac{dt}{4\pi} t \sum_\ell \left[\nu_\ell(t) - \nu_\ell^{(1)}(t) - \nu_\ell^{(2)}(t) - \dots - \nu_\ell^{(N)}(t) \right] + E_{\text{FD}}^{(N)} + E_{\text{CT}}. \quad (48)$$

B. Jost function for scattering about the vortex

The singularity of the vortex at its center makes it impossible to straightforwardly apply the standard form of the spectral methods described above. We will explain the required modifications in this section. The ultra-violet singularities that occur at third and higher order in the expansion of the effective action cancel (when regularized in a gauge invariant scheme). We may thus set $N = 2$ hereafter.

We return to the dimensionless variable $\rho = evr$ and $q = k/ev$ that enter the wave-equations (18). The scattering problem leads to the Jost solution by introducing $\Psi_\ell \sim \begin{pmatrix} \eta_\ell \\ a_{\ell+1} \end{pmatrix}$ in scattering channel ℓ as a 2×2 matrix with the free solution factored out,

$$\Psi_\ell = \mathcal{F}_\ell \cdot \mathcal{H}_\ell \quad \text{where} \quad \mathcal{H}_\ell = \begin{pmatrix} H_\ell^{(1)}(q\rho) & 0 \\ 0 & H_{\ell+1}^{(1)}(q\rho) \end{pmatrix}, \quad (49)$$

with boundary condition $\lim_{\rho \rightarrow \infty} \mathcal{F}_\ell = \mathbf{1}$. Since the two columns of \mathcal{H} represent free outgoing cylindrical waves for either η_ℓ or $a_{\ell+1}$, the scattering solution is

$$\Psi_\ell^{\text{sc}} = \mathcal{F}_\ell^* \cdot \mathcal{H}_\ell^* - \mathcal{F}_\ell \cdot \mathcal{H}_\ell \cdot \mathcal{S}_\ell$$

where \mathcal{S}_ℓ is the scattering matrix, which can be extracted using $\lim_{\rho \rightarrow 0} \Psi_{\text{sc}} = 0$. Then $\mathcal{F}_\ell(\rho, q)$ is the Jost solution, which leads to the Jost function $\mathcal{F}_\ell(q) = \lim_{\rho \rightarrow 0} \mathcal{F}_\ell(\rho, q)$. In both cases, $D = 2 + 1$ and $D = 3 + 1$, a major ingredient for the scattering piece of the VPE is the Jost function for imaginary momenta $\nu_\ell(t) = \ln \det [\mathcal{F}_\ell(it)]$. The angular momenta enter via the derivative matrix for the analytically continued Bessel functions

$$\mathcal{Z}_\ell = \begin{pmatrix} \frac{|\ell|}{\rho} - t \frac{K_{|\ell|+1}(t\rho)}{K_{|\ell|}(t\rho)} & 0 \\ 0 & \frac{|\ell+1|}{\rho} - t \frac{K_{|\ell+1|+1}(t\rho)}{K_{|\ell+1|}(t\rho)} \end{pmatrix} \quad \text{and} \quad \mathcal{L}_\ell = \begin{pmatrix} \ell^2 & 0 \\ 0 & (\ell+1)^2 \end{pmatrix}, \quad (50)$$

and the potential matrix is

$$\mathcal{V}_\ell = \begin{pmatrix} 3(h^2(\rho) - 1) + \frac{1}{\rho^2}(n^2 g^2(\rho) - 2n\ell g(\rho)) & \sqrt{2}d(\rho) \\ \sqrt{2}d(\rho) & 2(h^2(\rho) - 1) \end{pmatrix}. \quad (51)$$

In matrix form, the scattering differential equations read

$$\frac{\partial^2}{\partial \rho^2} \mathcal{F}_\ell = -\frac{\partial}{\partial \rho} \mathcal{F}_\ell - 2 \left(\frac{\partial}{\partial \rho} \mathcal{F}_\ell \right) \cdot \mathcal{Z}_\ell + \frac{1}{\rho^2} [\mathcal{L}_\ell, \mathcal{F}_\ell] + \mathcal{V}_\ell \cdot \mathcal{F}_\ell. \quad (52)$$

The standard procedure to determine the Born approximations, which are needed to regularize the ultraviolet divergences, terms fails when $g(0) \neq 0$ [26]. This can be seen by noting that the integral $\int_0^\infty \rho d\rho \left(\frac{g(\rho)}{\rho}\right)^2$, which would appear in the leading Born approximation in the gauge field potential, is ill-defined in the singular gauge. To perform the Born subtractions without the singular terms, we introduce

$$\bar{\mathcal{V}} = \begin{pmatrix} 3(h^2(\rho) - 1) & \sqrt{2}d(\rho) \\ \sqrt{2}d(\rho) & 2(h^2(\rho) - 1) \end{pmatrix} \quad (53)$$

and iterate the auxiliary differential equation

$$\frac{\partial^2}{\partial \rho^2} \bar{\mathcal{F}}_\ell = -\frac{\partial}{\partial \rho} \bar{\mathcal{F}}_\ell - 2 \left(\frac{\partial}{\partial \rho} \bar{\mathcal{F}}_\ell \right) \cdot \mathcal{Z}_\ell + \frac{1}{\rho^2} [\mathcal{L}_\ell, \bar{\mathcal{F}}_\ell] + \bar{\mathcal{V}} \cdot \bar{\mathcal{F}}_\ell \quad (54)$$

according to the expansion $\bar{\mathcal{F}}_\ell = \mathbf{1} + \bar{\mathcal{F}}_\ell^{(1)} + \bar{\mathcal{F}}_\ell^{(2)} + \dots$. The relevant leading orders are

$$\begin{aligned} \frac{\partial^2}{\partial \rho^2} \bar{\mathcal{F}}_\ell^{(1)} &= -\frac{\partial}{\partial \rho} \bar{\mathcal{F}}_\ell^{(1)} - 2 \left(\frac{\partial}{\partial \rho} \bar{\mathcal{F}}_\ell^{(1)} \right) \cdot \mathcal{Z}_\ell + \frac{1}{\rho^2} [\mathcal{L}_\ell, \bar{\mathcal{F}}_\ell^{(1)}] + \bar{\mathcal{V}}, \\ \frac{\partial^2}{\partial \rho^2} \bar{\mathcal{F}}_\ell^{(2)} &= -\frac{\partial}{\partial \rho} \bar{\mathcal{F}}_\ell^{(2)} - 2 \left(\frac{\partial}{\partial \rho} \bar{\mathcal{F}}_\ell^{(2)} \right) \cdot \mathcal{Z}_\ell + \frac{1}{\rho^2} [\mathcal{L}_\ell, \bar{\mathcal{F}}_\ell^{(2)}] + \bar{\mathcal{V}} \cdot \bar{\mathcal{F}}_\ell^{(1)}. \end{aligned} \quad (55)$$

All $\bar{\mathcal{F}}_\ell^{(m)}$ vanish in the limit $\rho \rightarrow \infty$. From the differential equations (52) and (55) we extract

$$\nu_\ell(t) = \lim_{\rho \rightarrow \rho_{\min}} \ln \det \mathcal{F}_\ell, \quad \bar{\nu}_\ell^{(1)}(t) = \lim_{\rho \rightarrow \rho_{\min}} \text{tr} \bar{\mathcal{F}}_\ell^{(1)} \quad \text{and} \quad \bar{\nu}_\ell^{(2)}(t) = \lim_{\rho \rightarrow \rho_{\min}} \text{tr} \left[\bar{\mathcal{F}}_\ell^{(2)} - \frac{1}{2} \left(\bar{\mathcal{F}}_\ell^{(1)} \right)^2 \right] \quad (56)$$

where ρ_{\min} is a tiny but nonzero number. The above expansion is the analog of Eq. (44) for the Jost function of the vortex with imaginary momentum.

The Jost functions for the ghost and fake boson are analogous to the above, but much simpler. The Jost solution is no longer a matrix, so the commutator term disappears. Then one just replaces \mathcal{V} and $\bar{\mathcal{V}}$ by $2v^2 [h^2(\rho) - 1]$ for the ghost and by $V_f(\rho)$ for the fake boson. Furthermore the angular momentum sum only involves non-negative values with a degeneracy factor two for $\ell \geq 1$.

By subtracting just $\bar{\nu}_\ell^{(1)}(t)$ and $\bar{\nu}_\ell^{(2)}(t)$ from $\nu_\ell(t)$ we do not include the subtractions for the singular terms that, in a gauge invariant formulation, induce a logarithmic ultra-violet divergence for $D = 3 + 1$. To investigate its relevance we compare the dimensional and sharp cut-off regularization schemes, leading to the identification (with an arbitrary mass scale M),

$$\frac{1}{\epsilon(4\pi)^2} = -i \int \frac{d^4 l}{(2\pi)^4} \frac{1}{(l^2 - M^2 + i0^+)^2} \Big|_{\text{div.}} = \frac{1}{8\pi^2} \int \frac{l^2 dl}{\sqrt{l^2 + M^2}^3} \Big|_{\text{div.}},$$

Together with the derivation of Eq. (36) we thus expect for $\rho_{\min} \rightarrow 0$

$$[\nu(t)]_V := \lim_{L \rightarrow \infty} \sum_{\ell=-L}^L \left[\nu_\ell(t) - \bar{\nu}_\ell^{(1)}(t) - \bar{\nu}_\ell^{(2)}(t) \right]_{\rho_{\min}} - n^2 \int_{\rho_{\min}}^\infty \frac{d\rho}{\rho} g^2(\rho) \xrightarrow{t \rightarrow \infty} \frac{n^2}{12t^2} \int_0^\infty \frac{d\rho}{\rho} \left(\frac{dg(\rho)}{d\rho} \right)^2. \quad (57)$$

Again, the superscripts denote the Born expansion order with respect to $\bar{\mathcal{V}}$. As explained in Ref. [26], the integral subtraction on the left hand side relates to a quadratic divergence in the VPE. By this subtraction we restore gauge invariance, which is not manifest for the Jost function. Note that we can write that integral as

$$n^2 \int_{\rho_{\min}}^\infty \frac{d\rho}{\rho} g^2(\rho) = \sum_\ell \int_{\rho_{\min}}^\infty \frac{d\rho}{\rho} J_\ell^2(qr) [n^2 g^2(\rho) - 2n\ell g(\rho)]$$

where the $J_\ell(z)$ are cylindrical Bessel functions. This shows that this integral replaces the leading Born approximation from the singular terms in the wave-equation. Its contribution to $\nu_\ell(t)$ arises from an integration by parts of an expression that contains its derivative with respect to t , cf. Eq. (43). Hence subtracting a constant times this quantity has no effect on the result, but renders the integral well-defined on the imaginary axis.

In $D = 3 + 1$ the right-hand-side of Eq. (57) leads to a logarithmic divergence that we computed in dimensional regularization in Eq. (36). It actually arises from a combination of two Feynman diagrams which individually are

quadratically divergent. The analogous Born expansion would indeed have to be performed individually. However, for the singular vortex configuration these integrals do not exist. Hence we apply the fake boson formalism developed in Ref. [27] and already described above. As shown in Eq. (40), the second-order term for a scalar field also yields a logarithmic divergence. In principle, the strength of that divergence does not depend on the mass of the boson. We take it to equal the Higgs/gauge mass so that we can simply subtract the associated Born term from $\nu_\ell(t)$ with a suitably adjusted strength and add it back as a Feynman diagram. To be precise, we consider scattering of a boson about the potential $V_f(\rho) = 3(\tanh^2(\kappa\rho) - 1)$, for which $\bar{\nu}_\ell^{(2)}(t)$ is the second-order contribution to the Jost function on the imaginary momentum axis. The partial wave expansion for this scalar field is similar to that of ghost field in Eq. (19) with $2(h(\rho) - 1)$ replaced by $V_f(\rho)$. We take κ as an arbitrary parameter to later test our numerical simulation, since the final result for VPE should not depend on a particular choice for V_f . This subtraction is calibrated by Eq. (41) which for the particular scalar potential reads

$$c_B = -\frac{e^2}{6} \frac{\int_0^\infty r dr F_{\mu\nu} F^{\mu\nu}}{\int_0^\infty r dr V_f^2} = -\frac{n^2}{3} \frac{\int_0^\infty \rho d\rho \left(\frac{g'(\rho)}{\rho}\right)^2}{\int_0^\infty \rho d\rho [3(\tanh^2(\kappa\rho) - 1)]^2}. \quad (58)$$

C. VPE for $D = 2 + 1$ and $D = 3 + 1$

For $D = 3 + 1$, the ghost and non-transverse gauge field contributions cancel. In that case, however, we still have to integrate over the momentum conjugate to the symmetry axis using the interface formalism finishing up with Eq. (48). For later discussion we separate the scattering contribution (including the factor of two for the complex fields) after the fake boson subtraction,

$$\frac{\Delta E_{\text{scat.}}}{(ev)^2} = \int_{\sqrt{2}}^\infty \frac{dt}{2\pi} t \{[\nu(t)]_V - c_B \nu_B(t)\}. \quad (59)$$

Here $\nu_B(t)$ is the angular momentum sum of the second Born contribution to the logarithm of the Jost function from the fake boson potential.

To evaluate the renormalized Feynman diagram contributions we introduce Fourier transforms of the vortex profiles

$$\begin{aligned} I_A(q) &= \int_0^\infty d\rho h(\rho) g(\rho) J_1(q\rho), & I_H(q) &= q \int_0^\infty \rho d\rho [1 - h(\rho)] J_0(q\rho), \\ \tilde{v}_H(q) &= \int_0^\infty \rho d\rho [h^2(\rho) - 1] J_0(q\rho), & \tilde{v}_f(q) &= 3 \int_0^\infty \rho d\rho [\tanh^2(\kappa\rho) - 1] J_0(q\rho), \end{aligned} \quad (60)$$

where, again, the $J_\ell(z)$ are cylindrical Bessel functions.

In $D = 3 + 1$ we have logarithmic divergences at second order, and we therefore separate the finite counterterm

$$\frac{E_{\text{CT}}}{e^2 v^2} = \int_0^\infty \rho d\rho \left\{ \frac{n^2}{144} \left(\frac{16}{\pi} - 3\sqrt{3} \right) \frac{g'^2}{\rho^2} + \left(\frac{1}{\pi} - \frac{1}{2\sqrt{3}} \right) \left[h'^2 + \frac{n^2}{\rho^2} h^2 g^2 + \frac{13}{8} (1 - h^2)^2 \right] \right\} \quad (61)$$

and the finite Feynman diagram contributions

$$\frac{E_{\text{FD}}}{e^2 v^2} = \frac{1}{\pi} \int_0^\infty dq \left[n^2 I_A^2(q) + I_H^2(q) + \frac{13}{8} \tilde{v}^2(q) + \frac{c_B}{8} \tilde{v}_f^2(q) \right] \left[\sqrt{q^2 + 8} \operatorname{asinh} \left(\frac{q}{\sqrt{8}} \right) - q \right]. \quad (62)$$

In $D = 2 + 1$ the second order contributions do not lead to an ultra-violet divergence. Nevertheless it is convenient to subtract them from the scattering data and add them back as Feynman diagrams because it allows us to use the same $[\nu(t)]_V$ as above. We separate the scattering contribution in Eq. (46) and need to augment it by the ghost piece

$$\frac{\Delta E_{\text{scat.}}}{ev} = \int_{\sqrt{2}}^\infty \frac{dt}{\pi} \frac{t}{\sqrt{t^2 - 2}} \{[\nu(t)]_V - c_B \nu_B(t)\} - \int_{\sqrt{2}}^\infty \frac{dt}{2\pi} \frac{t}{\sqrt{t^2 - 2}} \nu_{\text{gh}}(t), \quad (63)$$

where $\nu_{\text{gh}}(t)$ is the angular momentum sum of the logarithm of the Jost function with two Born subtractions for the single channel potential $V_{\text{gh}} = 2(\Phi_S^2 - v^2) = 2v^2(h^2(\rho) - 1)$. In comparison with Eq. (46), a factor of two again appears in the first integral because we are dealing with a complex boson field. Note that this first integral in Eq. (63) would also be finite without the fake boson subtraction. However, its inclusion improves the large momentum convergence of that integral and is thus advantageous in the numerical simulation.

The final ingredient is the renormalized Feynman diagram contribution in $D = 2 + 1$,

$$\begin{aligned} \frac{E_{\text{FD}}}{ev} = & \frac{n^2}{32\sqrt{2}} [\ln(27) - 4] \int_0^\infty \frac{d\rho}{\rho} g'^2(\rho) - \frac{c_B}{4} \int_0^\infty dq \tilde{v}_f^2(q) \arctan\left(\frac{q}{\sqrt{8}}\right) \\ & + \int_0^\infty dq \left[n^2 I_A^2(q) + I_H^2(q) + \frac{11}{8} \tilde{v}_H^2(q) \right] \left[\frac{\ln(3)}{\sqrt{2}} q - 2 \arctan\left(\frac{q}{\sqrt{8}}\right) \right]. \end{aligned} \quad (64)$$

As in Eq. (62) factors $1/\sqrt{2}$ emerged in the arguments of the trigonometric and hyperbolic functions in the counterterm contribution because $M = \sqrt{2}ev$.

VI. NUMERICAL RESULTS FOR THE VPE

We already reported some of the results for $D = 3 + 1$ in Ref. [12]. Unfortunately a sign error in c_h , corrected in Eq. (28), entered that earlier analysis and we take this opportunity to present the corrected data. The emerging changes are not significant enough to change any conclusion.

As a first step we substitute the profile functions with the parameterization of Eq. (9) into \mathcal{V} and $\bar{\mathcal{V}}$ in Eqs. (51) and (54), respectively. For a given angular momentum channel, we then integrate the differential equations (52) and (55) with the appropriate boundary conditions from a large $\rho_{\text{max}} \approx 20$ toward the center of the vortex to a small ρ_{min} . Once ρ_{min} is small enough, the extracted logarithms, Eq. (56) are stable with the exception of channels that do not have an angular momentum barrier at the center of the vortex. In those instances the regular and irregular solutions approach a constant and logarithm respectively, which are difficult to disentangle numerically. According to Eq. (18) these are the $\ell = -1$ and $\ell = n$ channels. In those channels we use several small values for ρ_{min} and fit

$$\ln \det \mathcal{F}_\ell - \bar{\mathcal{F}}_\ell^{(1)} - \bar{\mathcal{F}}_\ell^{(2)} - \frac{1}{2} \left(\bar{\mathcal{F}}_\ell^{(1)} \right)^2 = a_0 + \frac{a_1}{\ln(\rho_{\text{min}})} + \frac{a_2}{\ln^2(\rho_{\text{min}})}$$

where a_0 is the expression in square brackets in Eq. (57). This ρ_{min} extrapolation becomes more and more intricate with increasing winding n . Note that the $\ln(\rho_{\text{min}})$ singularity from the singular vortex arises from summing over arbitrarily large angular momenta. The above fit must also be performed for a regular gauge profile [28].

It is essential to verify that $[\bar{\nu}(t)]_V$ exhibits the asymptotic behavior suggested in Eq. (57) by the analysis of the two-point function for the gauge field. It turns out that even summing up to a large value like $L = 600$ is insufficient to compute the sum on the left-hand side. As explained in Ref. [26], on top of computing the sum for such large values of L an extrapolation for $L \rightarrow \infty$ is needed. This is done by using different large values of L in

$$\nu_L(t) = \sum_{\ell=-L}^L \left[\nu_\ell(t) - \bar{\nu}_\ell^{(1)}(t) - \bar{\nu}_\ell^{(2)}(t) \right]_{\rho_{\text{min}}} - n^2 \int_{\rho_{\text{min}}}^\infty \frac{d\rho}{\rho} g^2(\rho) \quad (65)$$

and extracting $[\nu(t)]_V$ from a fit of the form $\nu_L(t) \approx [\nu(t)]_V + \frac{b_1}{L} + \frac{b_2}{L^2}$. The importance of this extrapolation is shown in the inserts of Fig. 2. Though the numerical effect appears to be small, we note that the integrand for $D = 3 + 1$ in Eq. (59) has an additional factor of t , which amplifies any inaccuracy at large t . Also, without that extrapolation the integrand may incorrectly appear to converge without subtractions already at moderate t [26], which has led to incorrect conclusions in the past [15].

As suggested by this discussion, the numerical simulation is quite costly in computation time.³ We therefore compute $[\nu(t)]_V$ for about 200 different t values and implement a Laguerre interpolation to obtain a smooth function. This interpolation also allows for the substitution to $\tau = \sqrt{t^2 - 2}$, which avoids the integrable singularity in Eq. (63).

In Table II we present our results for the VPE of the vortex for $D = 2 + 1$. We also separate the ghost scattering contribution. Not surprisingly, this goes in the direction opposite to that of the Higgs and gauge bosons, but is more than an order of magnitude smaller when comparing the absolute values. We also list the Feynman diagram contribution from Eq. (64). There are significant cancellations between this and the scattering contribution. For $n = 1$ this cancellation is almost complete, while for larger winding numbers the total VPE is negative.

Table III contains our results for the VPE per unit length of the vortex in $D = 3 + 1$. Somewhat unexpectedly, the counterterm and Feynman diagram contributions go in the same direction, presumably because E_{CT} involves timelike

³ For large angular momenta sufficient accuracy can only be accomplished with *long-double* precision. This adds considerably to the computation time.

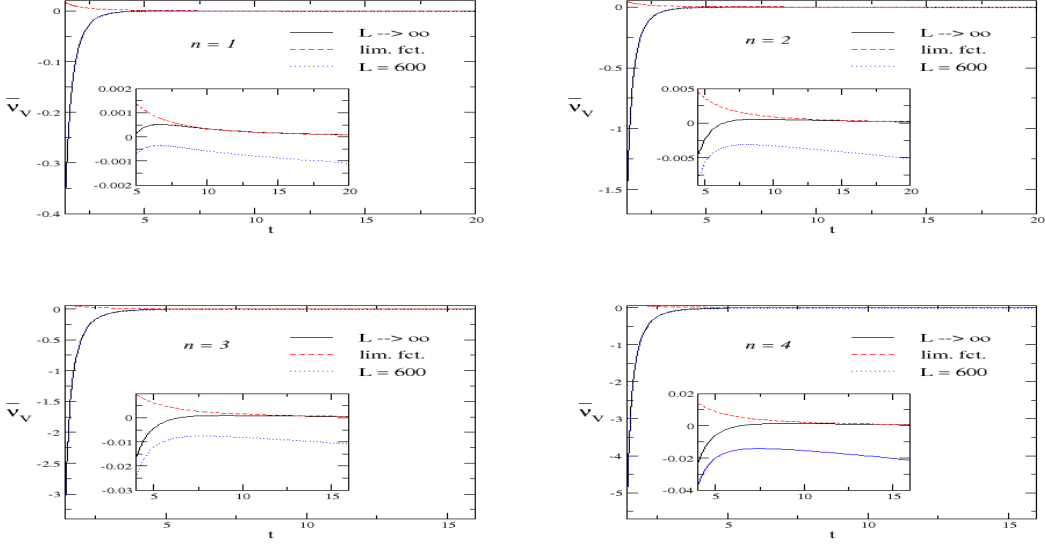


FIG. 2: Large angular momentum extrapolation from Eq. (65). The line labeled *lim.fct.* refers to the large t behavior in Eq.(57).

	$n = 1$	$n = 2$	$n = 3$	$n = 4$
$E_{\text{scat.}}^{(\text{H,A})}$	-0.1326	-0.5113	-0.9956	-1.5337
$E_{\text{scat.}}^{(\text{gh})}$	0.0078	0.0293	0.0579	0.0905
$\Delta E_{\text{scat.}}$	-0.1248	-0.4820	-0.9377	-1.4432
E_{FD}	0.1625	0.2455	0.3452	0.4504
ΔE	0.0377	-0.2365	-0.5925	-0.9928

TABLE II: Various contributions to the VPE of BPS vortices in $D = 2 + 1$ dimensions. The entries $E_{\text{scat.}}^{(\text{H,A})}$ and $E_{\text{scat.}}^{(\text{gh})}$ refer to the two integrals in Eq. (63). We use $\kappa = 1 - (n - 1)/10$ for the parameter of the fake boson potential $V_f(\rho)$. All data are in units of ev .

momenta while E_{FD} is an integral over spacelike momenta. Again there is a substantial cancellation between the scattering and Feynman diagram contributions once they are combined with the counterterms that implement the on-shell renormalization. In both cases ($D = 2 + 1$ and $D = 3 + 1$) $\Delta E_{\text{scat.}}$ is sizable. This is a clear indication that the VPE cannot be reliably computed from only low order Feynman diagrams.

In $D = 3 + 1$ the VPE is essentially linear in the winding number n . We fit the data from table III as: $\Delta E = 0.031 - 0.118(n - 1)$. The quality of the fit is measured as $\chi^2 = 2.7 \times 10^{-5}$. To obtain a similarly small $\chi^2 = 7.0 \times 10^{-5}$ in $D = 2 + 1$ we need to add a quadratic contribution $\Delta E = 0.040 - 0.250(n - 1) - 0.032(n - 1)^2$, even though the coefficient of that contribution is quite small.

We observe qualitatively similar winding number dependences in $D = 2 + 1$ and $D = 3 + 1$. An analogous similarity between these two cases was also found for the fermion VPE of QED flux tubes once equivalent renormalization conditions were implemented [29].

We have already performed a consistency test of our results when comparing the large momentum behavior of \bar{v}_V

	$n = 1$	$n = 2$	$n = 3$	$n = 4$
E_{CT}	0.0370	0.0786	0.1214	0.1651
E_{FD}	0.0424	0.0315	0.0317	0.0335
	0.0795	0.1101	0.1531	0.1986
$\Delta E_{\text{scat.}}$	-0.0510	-0.1939	-0.3563	-0.5251
ΔE	0.0284	-0.0837	-0.2033	-0.3257

TABLE III: Various contributions to the VPE of BPS vortices in $3 + 1$ dimensions: E_{CT} and E_{FD} are from Eqs. (61) and (62), respectively while $\Delta E_{\text{scat.}}$ is obtained from Eq. (59). The κ parameters are as in table II. All data are in units of $(ev)^2$.

	$\kappa = 0.7$	$\kappa = 1.0$		$\kappa = 0.7$	$\kappa = 1.0$
$E_{\text{scat.}}^{(\text{H,A})}$	-1.5337	-1.5316	E_{CT}	0.1651	0.1651
$E_{\text{scat.}}^{(\text{gh})}$	0.0905	0.0905	E_{FD}	0.0335	0.0326
$\Delta E_{\text{scat.}}$	-1.4432	-1.4414		0.1986	0.1977
E_{FD}	0.4504	0.4486	$\Delta E_{\text{scat.}}$	-0.5251	-0.5243
ΔE	-0.9928	-0.9928	ΔE	-0.3257	-0.3257

TABLE IV: Dependence of components of the VPE on the fake boson parameter κ for $n = 4$. Left panel: $D = 2 + 1$, right panel: $D = 3 + 1$.

in figure 2. We have also verified the independence with respect to the fake boson potential $V_f(\rho)$ by using different values for the mass parameter κ . We show an example in table IV with two κ values for $n = 4$ for both $D = 2 + 1$ and $D = 3 + 1$. Of course, the entries for $\kappa = 0.7$ are those from tables II and III. The variation with κ of the individual components is actually small. However, they are clearly visible and when combined to ΔE these variations indeed cancel.

Our results for the scattering data contributions $\Delta E_{\text{scat.}}$ generally agree with those of Ref. [14], in particular on the sign and the tendency with increasing winding number n . Those authors employed a truncated heat kernel expansion with ζ -function regularization. This amounts to an $\overline{\text{MS}}$ renormalization scheme and we have thus compared their results to $\Delta E_{\text{scat.}}$. However, our data are somewhat smaller in magnitude. We also agree with the sign in the prediction presented⁴ in Ref. [13] for $n = 1$ and $D = 3 + 1$. We also reproduce the significant cancellation between scattering and Feynman diagram contributions. Ref. [13] constructs the Greens function at coincident points from scattering data along the imaginary momentum axis. So it is essentially equivalent to ours. Nevertheless our results are smaller in magnitude. This may be due to the quality of the important angular momentum extrapolation. They extrapolate from $L \approx 35$ which is insufficient [26]. Also that Greens function approach requires an additional integral over the radial coordinate which maybe a source of numerical inaccuracies.

VII. CONCLUSIONS

We have computed the one-loop quantum corrections to the energy (per unit length) of ANO vortices in scalar electrodynamics with spontaneous symmetry breaking in the BPS case where the masses of the scalar and gauge fields are equal. These corrections arise from the polarization of the spectrum of quantum fluctuations in the classical vortex background. This vacuum polarization energy is small because the small coupling approximation applies to electrodynamics with $e^2 = 4\pi/137 \approx 0.09$, but, it becomes decisive for observables that are not sensitive to the classical energy, such as the binding energies of vortices with higher winding numbers in the BPS case, for which the classical result vanishes.

After clarifying a number of technical and numerical subtleties, we found that the dominant contribution to vacuum polarization energies of vortices stems from the non-perturbative contribution, which cannot be computed from the lowest order Feynman diagrams.⁵ Our numerical simulations for vortices with winding number up to four suggest that the quantum energy weakly binds higher winding number BPS vortices. We have also seen that the vacuum polarization energy for the unit winding number vortex is very small, so that at first glance it appears to be compatible with zero up to numerical errors. The potentially most important source for such errors is the small radius behavior in channels that contain zero angular momentum components. However, our numerical analysis suggests that any improvement of the data is small and likely to push that vacuum polarization energy further away from zero.

To our knowledge these are pioneering studies of a static soliton vacuum polarization energy that compare different topological sectors in a renormalizable model. This vortex model essentially has two space dimensions. Solitons in one space dimension do either not have topologically distinct⁶ static solitons, such as the kink and sine-Gordon soliton [30], or are destabilized by the quantum corrections, such as the ϕ^6 model soliton [31]. The Skyrme model [32] in three space dimensions indeed has static solitons with different winding numbers, but unfortunately that model is not renormalizable.

⁴ The erratum to Ref. [13] has a sign change compared to the original publication.

⁵ These diagrams represent an expansion in the background fields rather than the coupling constant.

⁶ There are different topological sectors in these models but the corresponding solitons solutions are constructed from those with the lowest nonzero winding number. For example, the $n = 2$ sine-Gordon solution is the superposition of two (infinitely) widely separated $n = 1$ solutions.

For $D = 2 + 1$ and $D = 3 + 1$ the VPE (approximately) decreases linearly with the winding number n with some offset at $n = 0$. For the binding energies $\Delta E - n\Delta E|_{n=1}$ we get $-0.290(n - 1) - 0.032(n - 1)^2$ and $-0.149(n - 1)$, respectively. Since in the BPS case the classical binding energy is strictly zero, this implies that it is energetically favorable for vortices to coalesce rather than to appear in isolation, as is characteristic of a type I superconductor. We also observe that $\Delta E|_{n=4} - 2\Delta E|_{n=2} < 0$, making the existence of substructures unlikely.

Away from the BPS case, the classical binding energy can quickly overwhelm the quantum correction since the model is weakly coupled. Nevertheless, the computation of their vacuum polarization energies for unequal masses would be desirable to complete this picture. Technically this calculation is more involved because it corresponds to a full 4×4 scattering problem, rather than a doubled 2×2 problem. Another interesting question is whether the techniques to avoid divergences in the Fourier transform of the vortices that was developed in Ref. [26] and employed here will also be successful when coupling fermions and thus avoid the implementation of a *return flux* [29]. If this is the case, supersymmetric extensions [33] can be investigated. We conjecture that analogous calculations are possible in the case of a 't Hooft-Polyakov monopole [34, 35].

Acknowledgments

N. G. is supported in part by the National Science Foundation (NSF) through grant PHY-1820700. H. W. is supported in part by the National Research Foundation of South Africa (NRF) by grant 109497.

-
- [1] A. A. Abrikosov, Sov. Phys. JETP **5**, 1174 (1957).
 - [2] A. A. Abrikosov, Journal of Physics and Chemistry of Solids **2**, 199 (1957).
 - [3] H. B. Nielsen and P. Olesen, Nucl. Phys. B **61**, 45 (1973).
 - [4] M. Tinkham, *Introduction to Superconductivity* (Dover, Mineola, New York, 1996).
 - [5] Y. Nambu, Nucl. Phys. B **130**, 505 (1977).
 - [6] T. W. B. Kibble, J. Phys. A **9**, 1387 (1976).
 - [7] E. P. S. Shellard and A. Vilenkin, *Cosmic Strings and Other Topological Defects* (Cambridge University Press, Cambridge, UK, 1994).
 - [8] E. B. Bogomolny, Sov. J. Nucl. Phys. **24**, 449 (1976).
 - [9] M. K. Prasad and C. M. Sommerfield, Phys. Rev. Lett. **35**, 760 (1975).
 - [10] N. Graham and H. Weigel, Int. J. Mod. Phys. A **37**, 2241004 (2022), 2201.12131.
 - [11] N. Graham, M. Quandt, and H. Weigel, *Spectral Methods in Quantum Field Theory*, vol. 777 (Springer-Verlag, Berlin, 2009).
 - [12] N. Graham and H. Weigel, Phys. Rev. **D104**, 011901 (2021).
 - [13] J. Baacke and N. Kevlishvili, Phys. Rev. **D78**, 085008 (2008), [Erratum: Phys. Rev. D **82**, 129905 (2010)].
 - [14] A. Alonso-Izquierdo, J. Mateos Guilarte, and M. de la Torre Mayado, Phys. Rev. D **94**, 045008 (2016).
 - [15] P. Pasipoularides, Phys. Rev. **D64**, 105011 (2001).
 - [16] N. Graham, R. L. Jaffe, M. Quandt, and H. Weigel, Phys. Rev. Lett. **87**, 131601 (2001).
 - [17] A. Rebhan, P. van Nieuwenhuizen, and R. Wimmer, Braz. J. Phys. **34**, 1273 (2004).
 - [18] B.-H. Lee and H. Min, Phys. Rev. D **51**, 4458 (1995).
 - [19] C. Becchi, A. Rouet, and R. Stora, Commun. Math. Phys. **42**, 127 (1975).
 - [20] N. Irges and F. Koutroulis, Nucl. Phys. B **924**, 178 (2017), [Erratum: Nucl. Phys. B **938**, 957–960 (2019)].
 - [21] J. S. Faulkner, J. Phys. **C10**, 4661 (1977).
 - [22] F. Calegiero, *Variable Phase Approach to Potential Scattering* (Academic Press, New York, 1967).
 - [23] R. G. Newton, *Scattering Theory of Waves and Particles* (Springer, New York, 1982).
 - [24] M. Bordag and K. Kirsten, Phys. Rev. **D53**, 5753 (1996).
 - [25] N. Graham, R. L. Jaffe, M. Quandt, and H. Weigel, Annals Phys. **293**, 240 (2001).
 - [26] N. Graham and H. Weigel, Phys. Rev. **D101**, 076006 (2020).
 - [27] E. Farhi, N. Graham, R. L. Jaffe, and H. Weigel, Nucl. Phys. B **630**, 241 (2002).
 - [28] N. Graham, M. Quandt, and H. Weigel, Phys. Rev. D **84**, 025017 (2011), 1105.1112.
 - [29] N. Graham, V. Khemani, M. Quandt, O. Schröder, and H. Weigel, Nucl. Phys. B **707**, 233 (2005).
 - [30] R. Rajaraman, *Solitons and Instantons* (North Holland, Amsterdam, 1982).
 - [31] H. Weigel, AIP Conf. Proc. **2116**, 170002 (2019).
 - [32] T. H. R. Skyrme, Proc. Roy. Soc. Lond. A **260**, 127 (1961).
 - [33] J. D. Edelstein, C. Nunez, and F. Schaposnik, Phys. Lett. B **329**, 39 (1994).
 - [34] G. 't Hooft, Nucl. Phys. B **79**, 276 (1974).
 - [35] A. M. Polyakov, JETP Lett. **20**, 194 (1974).